Journal of Solid State Chemistry 181 (2008) 3095–3102

Contents lists available at ScienceDirect

Journal of Solid State Chemistry

journal homepage: www.elsevier.com/locate/jssc

La^{3+} doping of the Sr_2CoWO_6 double perovskite: A structural and magnetic study

C.A. López [a], M.C. Viola [a], J.C. Pedregosa [a,*], R.E. Carbonio [b], R.D. Sánchez [c], M.T. Fernández-Díaz [d]

[a] Área de Química General e Inorgánica "Dr. Gabino F. Puelles", Departamento de Química, Facultad de Química, Bioquímica y Farmacia, Universidad Nacional de San Luis, Chacabuco y Pedernera, 5700 San Luis, Argentina

[b] Departamento de Fisicoquímica, Facultad de Ciencias Químicas, Instituto de Investigaciones en Físico Química de Córdoba (INFIQC) CONICET, Universidad Nacional de Córdoba, Ciudad Universitaria, 5000 Córdoba, Argentina

[c] Instituto Balseiro, Universidad Nacional de Cuyo and Centro Atómico Bariloche, Comisión Nacional de Energía Atómica, 8400 S.C. de Bariloche, Río Negro, Argentina

[d] Institut Laue-Langevin, B.P. 156, F-38042 Grenoble Cedex 9, France

ARTICLE INFO

Article history:
Received 25 April 2008
Received in revised form
11 July 2008
Accepted 5 August 2008
Available online 17 August 2008

Keywords:
Sr_2CoWO_6
Double perovskite
La doped
Structure
Magnetic behavior

ABSTRACT

La-doped Sr_2CoWO_6 double perovskites have been prepared in air in polycrystalline form by solid-state reaction. These materials have been studied by X-ray powder diffraction (XRPD), neutron powder diffraction (NPD) and magnetic susceptibility. The structural refinement was performed from combined XRPD and NPD data (D2B instrument, $\lambda = 1.594$ Å). At room temperature, the replacement of Sr^{2+} by La^{3+} induces a change of the tetragonal structure, space group $I4/m$ of the undoped Sr_2CoWO_6 into the distorted monoclinic crystal structure, space group $P2_1/n$, $Z = 2$. The structure of La-doped phases contains alternating CoO_6 and $(Co/W)O_6$ octahedra, almost fully ordered. On the other hand, the replacement of Sr^{2+} by La^{3+} induces a partial replacement of W^{6+} by Co^{2+} into the B sites, i.e. $Sr_{2-x}La_xCoW_{1-y}Co_yO_6$ ($y = x/4$) with segregation of $SrWO_4$. Magnetic and neutron diffraction measurements indicate an antiferromagnetic ordering below $T_N = 24$ K independently of the La-substitution.

1. Introduction

Since the discovery of colossal magnetoresistance (CMR) in manganites there was an increasing interest of solid-state chemists and physicists to prepare new compounds that could have this property, since this effect is of technological interest for the detection of magnetic fields in magnetic memory devices. A few years ago, a report about Sr_2FeMoO_6 [1] demonstrating that in its electronic structure only minority spins are present at the Fermi level and that it exhibited intrinsic tunneling-type magnetoresistance (TMR) at room temperature (RT) motivated the study of this material [2,3] and triggered the interest to prepare new double perovskites which potentially could present half-metallic properties.

We recently reported the induction of CMR in Sr_2CoMoO_6 [4] upon chemical reduction, via topotactical removal of oxygen atoms. We also prepared Sr_2CoWO_6 [5]. At RT, the crystal structure was tetragonal, space group $I4/m$, with $a = 5.58277(1)$ Å and $c = 7.97740(1)$ Å. The structure contains alternating CoO_6 and WO_6 octahedral units, tilted in anti-phase by 7.24° in the basal ab plane along the [001] direction of the pseudocubic cell. This corresponds to the $a^0a^0c^-$ Glazer's notation as derived by Woodward for 1:1 ordering of double perovskites [6], consistent with space group $I4/m$. Magnetic and neutron diffraction measurements indicate an antiferromagnetic ordering below $T_N = 24$ K. Magnetic and electrical properties and bond valence sums are consistent with the electronic configuration $Co^{2+}(3d^7)$–$W^{6+}(5d^0)$.

Based on our findings with Sr_2CoWO_6 we tried to induce semiconductivity and magnetotransport by chemical reduction in this compound, but we were unsuccessful, probably due to the difficulty in reducing W^{6+}. Another possibility is to induce semiconductivity by electron doping replacing Sr^{2+} in the A site by a trivalent cation [7–9]. It has been previously reported that the replacement of A^{2+} by Ln^{3+} in $A_2FeB''O_6$ (where $B'' = Mo$) induces magnetic and structural changes [10]. When doping with La, an important fraction of the injected electrons is localized at Mo sites, which is harmful concerning the potential applicability, since it promotes the occurrence of anti-site disordering between Fe and Mo cations [11–13]. There are no previous studies about electron doping with Co and W containing double perovskites, for these reasons, it is interesting to study La^{3+} doping in Sr_2CoWO_6.

* Corresponding author. Fax: +54 2652 430224.
E-mail address: jpedreg@unsl.edu.ar (J.C. Pedregosa).

0022-4596/$ - see front matter © 2008 Elsevier Inc. All rights reserved.
doi:10.1016/j.jssc.2008.08.007

In the present work we describe the synthesis of La(III)-doped Sr_2CoWO_6 double perovskites prepared by a solid-state reaction and the results of Rietveld analysis of X-ray powder diffraction (XRPD) and neutron powder diffraction (NPD) data on a well-crystallized sample. Crystal and magnetic structures for these compounds as a function of La doping are discussed. Macroscopic magnetic measurements are also presented.

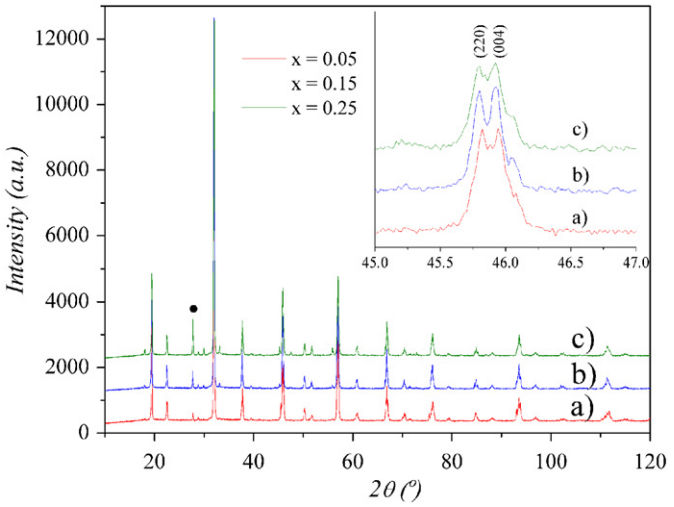

Fig. 1. XRPD patterns for La-doped double perovskites at RT: (a) SL05, (b) SL15 and (c) SL25. The circle indicates the main reflection of the $SrWO_4$ impurity phase. The inset shows the splitting of the (004) reflections corresponding to the cubic space group $Fm\bar{3}m$, typical of a monoclinic distortion.

2. Experimental

$Sr_{2-x}La_xCoWO_6$ double perovskites with nominal $x = 0.05$ (SL05), 0.15 (SL15) and 0.25 (SL25) were prepared as brown polycrystalline powders by a solid-state reaction. Stoichiometric amounts of analytical grade $SrCO_3$, La_2O_3, $CoCO_3$ and WO_3 were mixed, ground, placed in a platinum crucible and treated at 600 °C in air for 12 h. The resulting powder was reground and calcined at 900 °C for 12 h. Finally the product was fired at 1150 °C in three periods totaling 48 h with intermediate milling of the reaction mixture. The rate of heating was of 5 °C min^{-1}. The general proposed reaction is

$$(2-x)\ SrCO_3 + (x/2)\ La_2O_3 + CoCO_3 + WO_3 \rightarrow Sr_{2-x}La_xCoWO_6 + ((2-x)+1)CO_2 + x/4\ O_2$$

where nominal $x = 0.05$, 0.15, 0.25.

The initial structural identification and characterization of the samples was carried out by XRPD. The XRPD patterns (Cu$K\alpha$, $\lambda = 1.5418$ Å) (Fig. 1) are characteristic of a perovskite structure,

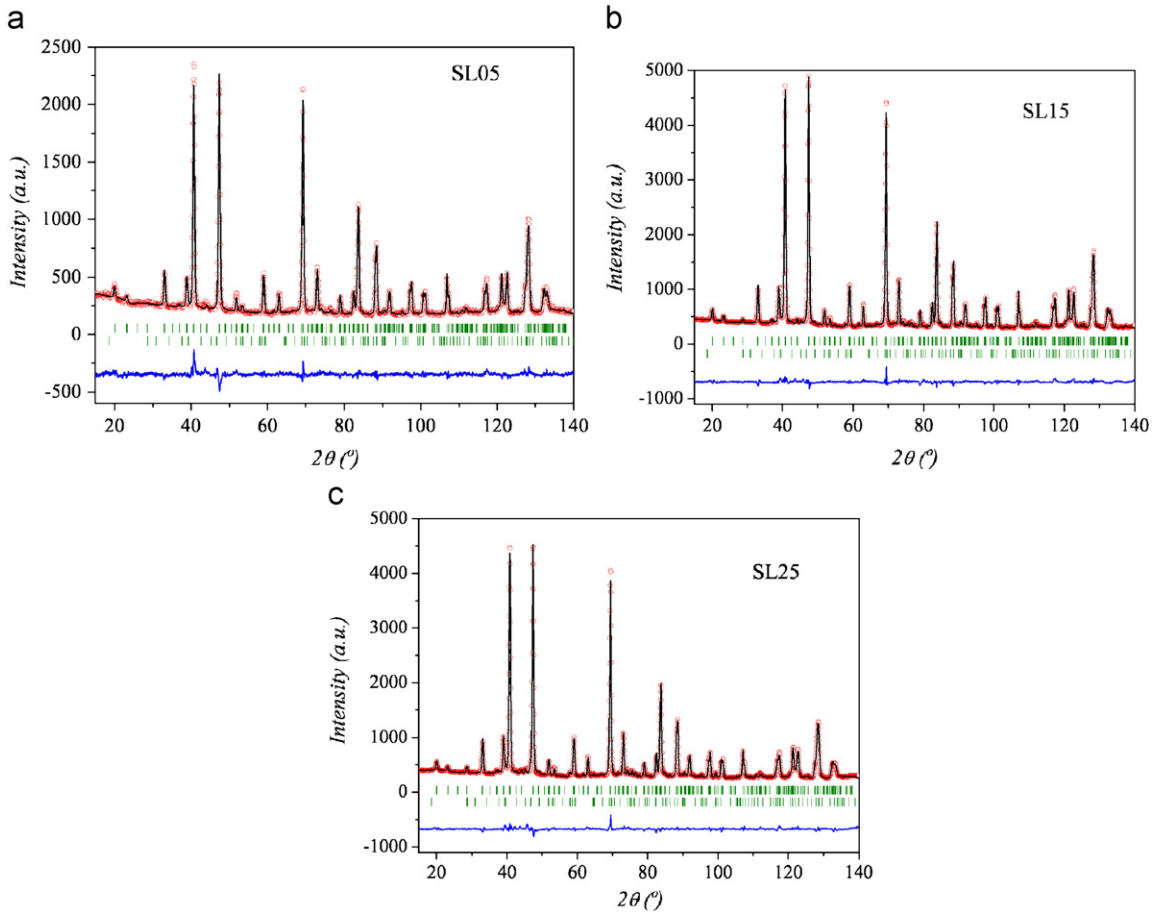

Fig. 2. Observed (circles), calculated (full line) and difference (bottom) high-resolution NPD Rietveld profiles at RT for La-doped double perovskites at RT for (a) SL05, (b) SL15 and (c) SL25; the upper set of bars corresponds to the Bragg reflections for the main phase and the lower set of bars corresponds to the Bragg reflections for the $SrWO_4$ impurity phase.

showing the splitting of certain reflections, typical of a monoclinic distortion, for instance, the (004) reflection of the prototype cubic ($Fm\bar{3}m$ space group). Minor amounts of $SrWO_4$ were detected from either XRPD or NPD data.

The magnetic measurements were performed in a commercial SQUID magnetometer. The susceptibility was measured in field cooling conditions under a 1000 Oe magnetic field, for temperatures ranging from 4 to 315 K.

To study the crystallographic structure, NPD patterns were collected at RT, 200, 100, 50 and 5 K on the D2B diffractometer (ILL, Grenoble) with a wavelength of 1.594 Å.

NPD and XRPD patterns were refined with the Rietveld method [14] using the FULLPROF program [15]. In the refinements, the shape of the peaks was simulated by a pseudo-Voigt function and the background was fitted by a fifth-degree Chebyshev polynomial. The coherent scattering lengths for Sr, La, Co, W and O were 8.24, 7.02, 2.5, 4.77 and 5.805 fm, respectively. The minor $SrWO_4$ impurity (with a scheelite structure) was included as a second crystallographic phase in the refinements. In the final runs, the following parameters were refined: scale factors for the main and impurity phases, background coefficients, zero-point error, unit-cell parameters, pseudo-Voigt correction for asymmetric parameters, positional coordinates, isotropic atomic displacement parameters, and relative Sr/La and Co/W occupancy factors.

3. Results and discussion

3.1. Crystallographic structure

Unlike the Sr_2CoWO_6 which presents tetragonal $I4/m$ symmetry [5] in these doped compounds the Bragg reflections were indexed with a monoclinic unit cell and the structure was refined in the space group $P2_1/n$ (monoclinic, no. 14, non-standard setting) (unique axis b, cell choice 2 [16]). Sr and La atoms were located at 4*e* (*x*,*y*,*z*) positions, Co at 2*c* (1/2,0,1/2) and Co/W at 2*d* (1/2,0,0) sites, and oxygen atoms at 4*e* (*x*,*y*,*z*). $SrWO_4$ was included in the refinement as a second phase, defined in the tetragonal space group $I4_1/a$ [17]. From the scale factor of the main and secondary phases we estimated the following impurity levels as wt%: 0.9(1)%, 4.7(2)% and 6.5(3)% of $SrWO_4$ for samples SL05, SL15 and SL25, respectively. An excellent fit was obtained for this model. The differences with the same other models are very subtle since they involve mainly small shifts of the in-plane oxygen atoms. These position changes can be difficult to detect by XRPD; hence, an NPD study is essential for investigation of these structural features since neutrons are more sensitive to the oxygen positions. Our RT NPD study performed at the D2B diffractometer allowed us to determine the true space group: a trial refinement in other space groups led to a much worse fit of the data. Also, as shown in Fig. 1 (inset), the splitting can be

Table 1
Positional, isotropic atomic displacement parameters, and occupancies for La-doped double perovskites $[Sr_{2-x}La_x]_{4e}[Co]_{2c}[W_{1-y}Co_y]_{2d}O_6$ in the monoclinic $P2_1/n$ space group, $Z = 2$, from NPD and XRPD data at 298 K

Atoms	*x*/*a*	*y*/*b*	*z*/*c*	Biso	Occ.
(a) $[Sr_{1.94}La_{0.06}]_{4e}[Co]_{2c}[W_{0.984}Co_{0.016}]_{2d}O_6$ (SL05)[a]					
Sr 4*e*	1.000(1)	1.007(1)	0.250(1)	1.00(3)	0.969(9)
La 4*e*	1.000(1)	1.007(1)	0.250(1)	1.00(3)	0.031(9)
Co 2*c*	0.5	0	0.5	0.3(1)	1.000
W 2*d*	0.5	0	0	1.13(5)	0.984(4)
Co 2*d*	0.5	0	0	1.13(5)	0.016(4)
O1 4*e*	1.048(1)	0.496(2)	0.261(1)	0.87(9)	1.000
O2 4*e*	0.729(1)	0.255(1)	1.024(2)	1.27(2)	1.000
O3 4*e*	0.245(1)	0.227(1)	0.978(2)	1.09(2)	1.000
NPD discrepancy factors: R_p: 14.3%; R_{wp}: 11.8%; R_{exp}: 8.61%; χ^2: 1.89					
XRPD discrepancy factors: R_p: 9.96%; R_{wp}: 7.35%; R_{exp}: 10.91%; χ^2: 0.453					
(b) $[Sr_{1.86}La_{0.14}]_{4e}[Co]_{2c}[W_{0.964}Co_{0.036}]_{2d}O_6$ (SL15)[b]					
Sr 4*e*	0.9991(4)	1.0104(5)	0.2498(8)	1.32(2)	0.93(1)
La 4*e*	0.9991(4)	1.0104(5)	0.2498(8)	1.32(2)	0.07(1)
Co 2*c*	0.5	0	0.5	0.8(1)	1.000
W 2*d*	0.5	0	0	0.56(6)	0.964(6)
Co 2*d*	0.5	0	0	0.56(6)	0.036(6)
O1 4*e*	1.0484(3)	0.4975(6)	0.2606(6)	1.14(5)	1.000
O2 4*e*	0.7227(6)	0.2591(8)	1.0273(6)	1.51(9)	1.000
O3 4*e*	0.2448(7)	0.2281(7)	0.9783(6)	1.39(8)	1.000
NPD discrepancy factors: 7.74%; R_{wp}: 7.15%; R_{exp}: 3.02%; χ^2: 5.62					
XRPD discrepancy factors: R_p: 13.4%; R_{wp}: 10.1%; R_{exp}: 11.20%; χ^2: 0.820					
(c) $[Sr_{1.82}La_{0.18}]_{4e}[Co]_{2c}[W_{0.956}Co_{0.044}]_{2d}O_6$ (SL25)[c]					
Sr 4*e*	0.9995(4)	1.0065(8)	0.2502(9)	1.57(2)	0.91(1)
La 4*e*	0.9995(4)	1.0065(8)	0.2502(9)	1.57(2)	0.09(1)
Co 2*c*	0.5	0	0.5	0.8(2)	1.000
W 2*d*	0.5	0	0	1.00(9)	0.956(6)
Co 2*d*	0.5	0	0	1.00(9)	0.044(6)
O1 4*e*	1.0496(4)	0.4972(9)	0.2594(7)	1.24(5)	1.000
O2 4*e*	0.7405(9)	0.2489(8)	1.0207(8)	1.85(9)	1.000
O3 4*e*	0.2289(8)	0.2216(8)	0.9726(7)	1.37(8)	1.000
NPD discrepancy factors: R_p: 7.78; R_{wp}: 7.56; R_{exp}: 2.75; χ^2: 7.53					
XRPD discrepancy factors: R_p: 14.7; R_{wp}: 11.6; R_{exp}: 11.81; χ^2: 0.963					

Reliability factors after the Rietveld refinement are also given.
[a] The unit cell parameters are $a = 5.6204(3)$ Å, $b = 5.5942(3)$ Å, $c = 7.9050(5)$ Å, $\beta = 90.033(7)^\circ$, $V = 248.55(3)$ Å^3.
[b] The unit cell parameters are $a = 5.6178(3)$ Å, $b = 5.5915(3)$ Å, $c = 7.9032(4)$ Å, $\beta = 90.039(4)^\circ$, $V = 248.25(2)$ Å^3.
[c] The unit cell parameters are $a = 5.6164(4)$ Å, $b = 5.5899(4)$ Å, $c = 7.8999(6)$ Å, $\beta = 90.005(6)^\circ$, $V = 248.02(3)$ Å^3.

correctly accounted by considering a monoclinic symmetry. $P2_1/n$ (no. 14, non-standard setting) (unique axis *b*, cell choice 2). In fact, this symmetry and space group are adopted by other related and well-known double perovskites [18], with small tolerance factors, such as Ca_2FeMoO_6 [19].

The structural refinement of SL05-, SL15- and SL25-doped double perovskites was performed from combined XRPD and NPD data at RT. The good agreement between the observed and calculated NPD patterns after the refinement is shown in Fig. 2.

Table 1 includes the final atomic coordinates and discrepancy factors after the refinement for La-doping phases at 298 K. Table 2 lists the main interatomic distances and angles. As can be seen there is a gradual decrease in cell parameters and in the mean distance ⟨*A*–O⟩ as doping with La^{3+} increases, consistent with the lower ionic radius of La^{3+} (1.36 Å) compared to Sr^{2+} (1.44 Å) (see Fig. 3). This smaller size of La^{3+} is responsible for the larger monoclinic distortion as doping increases.

In spite of the similarity of the neutron scattering lengths of Sr and La, an accurate value of the mixed Sr/La occupancy could be obtained from the combined refinement from XRPD and NPD data. We found La occupancies in the *A* site (4*e* Wyckoff position) were 3.1%, 7.0% and 9.0% for SL05, SL15 and SL25, respectively. These values are consistent with the amount of $SrWO_4$ that was found for the different proposed stoichiometries.

Occupancies in the *B* sites were also refined. In this case, besides the large difference in the X-rays scattering factors, there is also a large difference in the NPD scattering lengths between Co and W, so we can refine the *B* site occupancies with confidence. The good result is shown by the very low errors in these values, which are in the third decimal figure (see Table 1). The possibility of Co/W anti-site disordering, assuming that some Co from the 2*c* positions could randomly replace some W at 2*d* positions was also checked. The 2*c* site was always fully occupied by Co. On the other hand in the 2*d* site, Co occupancy increases as La doping increases, being 0.016, 0.036 and 0.044 for SL05, SL15 and SL25, respectively. The oxygen stoichiometry of O1, O2 and O3 was checked by refining their occupancy factors; no oxygen vacancies or oxygen excess were found to be present within the experimental error.

Table 2
Main bond distances (Å) and selected angles (deg) for monoclinic La-doped double perovskites $[Sr_{2-x}La_x]_{4e}[Co]_{2c}[W_{1-y}Co_y]_{2d}O_6$ from NPD and XRPD data at 298 K

	SL05	SL15	SL25
CoO_6 octahedra			
Co–O1 (× 2)	2.078(9)	2.077(5)	2.068(5)
Co–O2 (× 2)	2.056(8)	2.071(4)	2.030(5)
Co–O2 (× 2)	2.062(8)	2.057(4)	2.030(4)
⟨Co–O⟩	2.066(3)	2.069(2)	2.043(2)
$B''O_6$ octahedra			
B″–O1(× 2)	1.911(9)	1.912(5)	1.921(5)
B″–O2(× 2)	1.933(8)	1.926(4)	1.946(5)
B″–O3(× 2)	1.924(8)	1.926(4)	1.975(4)
⟨*B″*–O⟩	1.923(3)	1.921(2)	1.947(2)
Co–O1–*B″*(× 2)	164.4(4)°	164.3(2)°	163.9(2)°
Co–O2–*B″*(× 2)	167.5(3)°	165.1(2)°	170.4(2)°
Co–O3–*B″*(× 2)	168.0(3)°	168.3(2)°	163.2(2)°
⟨Co–O–*B″*⟩	166.6°	165.9°	165.8°
AO_{12} polyhedra			
A–O1	2.87(1)	2.882(4)	2.862(7)
A–O1	2.75(1)	2.740(4)	2.758(7)
A–O1	3.08(1)	3.078(3)	3.085(3)
A–O1	2.55(1)	2.544(3)	2.534(3)
A–O2	2.73(1)	2.727(6)	2.690(8)
A–O2	2.61(1)	2.575(6)	2.677(8)
A–O2	3.03(1)	3.084(7)	2.958(8)
A–O2	2.85(1)	2.837(7)	2.875(8)
A–O3	2.83(1)	2.828(7)	2.813(8)
A–O3	3.03(1)	3.029(7)	3.108(8)
A–O3	2.61(1)	2.627(6)	2.524(7)
A–O3	2.74(1)	2.729(6)	2.776(7)
⟨*A*–O⟩	2.81(1)	2.807(7)	2.805(7)

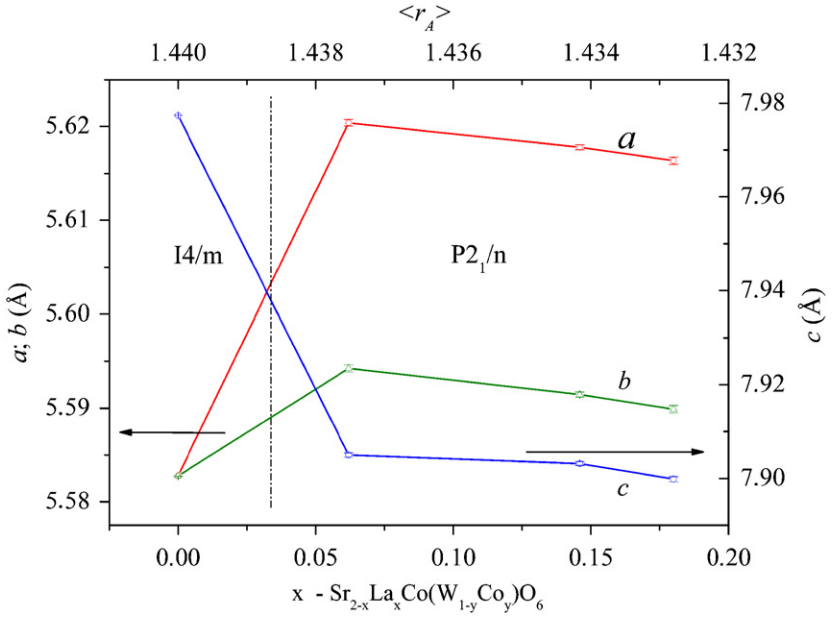

Fig. 3. Cell parameters evolution with La doping: (a) SL05, (b) SL15 and (c) SL25.

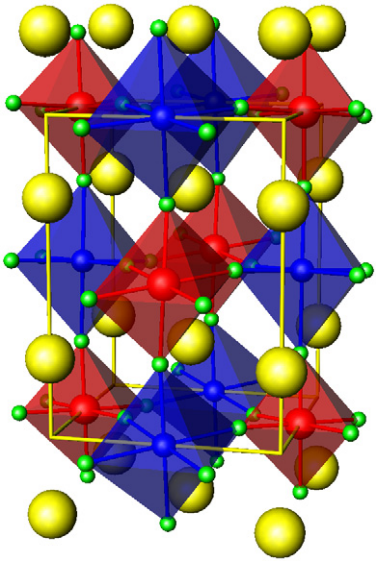

Fig. 4. A view of the crystal structure of the La-doped double perovskites; each CoO_6 octahedron is corner linked to six $B''O_6$ octahedra.

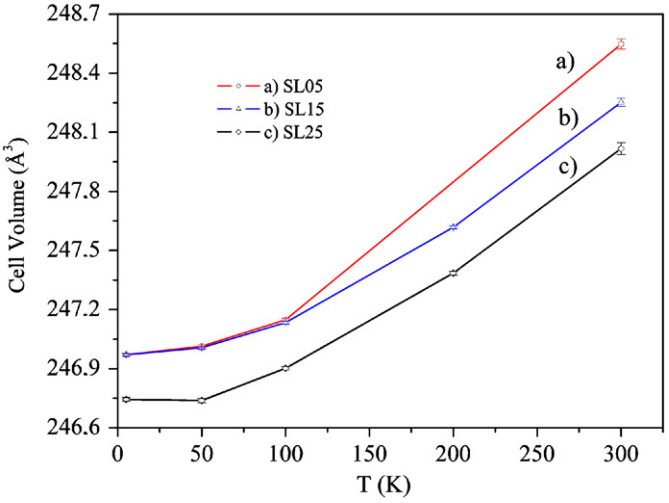

Fig. 5. Thermal evolution of the cell volume for La-doped double perovskites obtained from NPD: (a) SL05, (b) SL15 and (c) SL25.

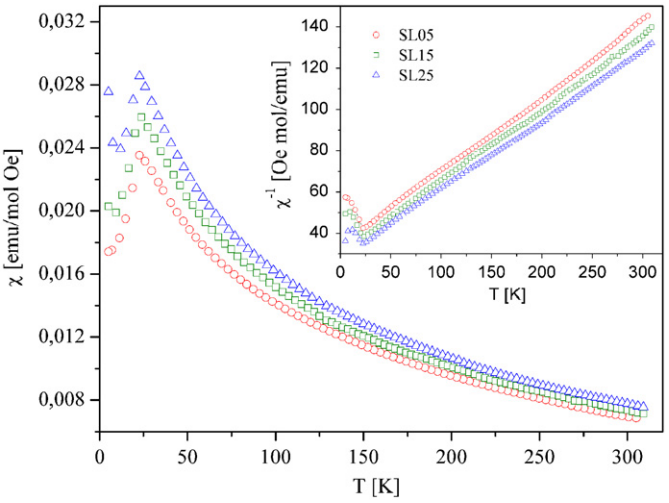

Fig. 6. Magnetic susceptibility as a function of temperature for La-doped double perovskites: (a) SL05, (b) SL15 and (c) SL25. Inset: reciprocal susceptibility vs. *T*.

These values explain the gradual increase in segregation of $SrWO_4$ as La doping increases and shows that the attempts to replacement Sr^{2+} by La^{3+} so as to reduce W^{6+} to W^{5+} and dope with electrons is not allowed, at least under these experimental conditions. There are no examples of W^{5+} double perovskites obtained in an air atmosphere, since the W^{5+} cation requires rather strong reducing conditions to be stabilized, which can be achieved by annealing at high temperatures (1000–1200 °C) in H_2/N_2 (or H_2/Ar) atmosphere (for instance Sr_2CrWO_6 [20]). As a consequence, in order to maintain electroneutrality, as La^{3+} is incorporated into the 4*e* Wyckoff site, a fraction of W^{6+} is replaced by Co^{2+} ions into the 2*d* Wyckoff sites.

As a consequence, real stoichiometries can be written as:

$[Sr_{1.94}La_{0.06}]_{4e}[Co]_{2c}[W_{0.984}Co_{0.016}]_{2d}O_6$ (for SL05)

$[Sr_{1.86}La_{0.14}]_{4e}[Co]_{2c}[W_{0.964}Co_{0.036}]_{2d}O_6$ (for SL15)

$[Sr_{1.82}La_{0.18}]_{4e}[Co]_{2c}[W_{0.956}Co_{0.044}]_{2d}O_6$ (for SL25)

Thus, we can write the general formula for these compounds as $[Sr_{2-x}La_x]_{4e}[Co]_{2c}[W_{1-y}Co_y]_{2d}O_6$ where $y = x/4$, and in the limit for $x = 2$ ($y = 0.5$) we should obtain $[La_2]_{4e}[Co]_{2c}[W_{0.5}Co_{0.5}]_{2d}O_6$. Although the major part of the initial amount of La occupies the *A* site, La_2O_3, as residue, remains in the samples and the corresponding diffraction peaks can be hardly observed since they are masked by the background. Although this fact has no influence on the refinement it could justify the difference in the stoichiometry between the target phases and the refined Sr/La rations.

A drawing of the structure is shown in Fig. 4; it contains alternating CoO_6 and $(Co,W)O_6$ octahedra, tilted in phase along the (100) direction of the pseudocubic cell and in anti-phase along the (010) and (001) directions, which corresponds to the $a^-a^-b^+$ Glazer's notation as derived by Woodward [6] for 1:1 ordering of double perovskites, consistent with space group $P2_1/n$. The average tilting angles can be estimated as $\varphi = (180^\circ - \theta)/2$, where $\theta = \langle$Co–O–$B''\rangle$; we obtain $\varphi = 6.7^\circ$, 7.0° and 7.1° for SL05, SL15 and SL25, respectively, clearly there is an increase in the tilting angle as La doping increases.

The thermal variation of the unit-cell parameters refined from NPD taken at 300, 200, 100, 50 and 5 K shows a decrease of cell volume (see Fig. 5). In the final refinement of the 5 K crystallographic structure we included a model for the magnetic structure, as described below.

3.2. Magnetic data

The magnetic susceptibility vs. temperature curves for SL05-, SL15- and SL25-doped double perovskites (Fig. 6) show a low-temperature maximum, at $T_N = 24$ K, corresponding to the transition to an antiferromagnetically ordered phase. The same

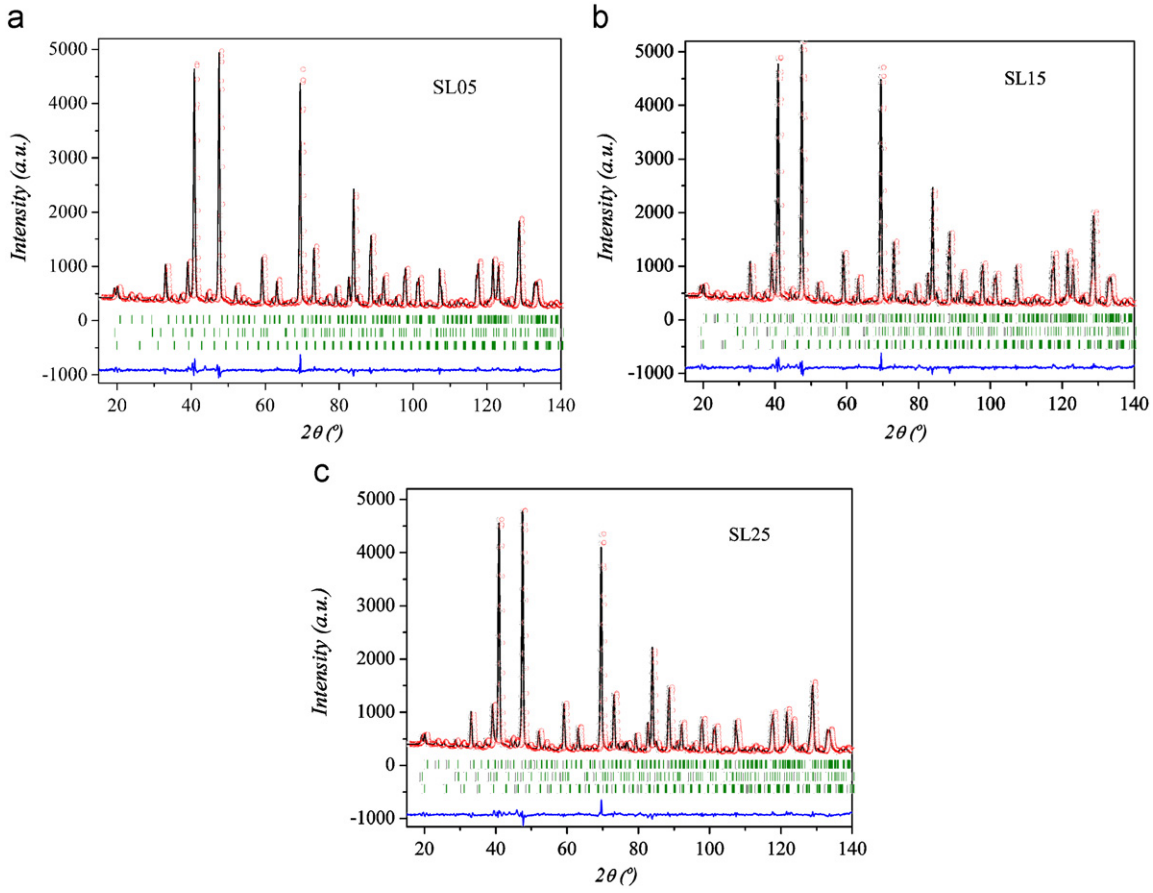

Fig. 7. Observed (circles), calculated (full line) and difference (bottom) high-resolution NPD Rietveld profiles for La-doped double perovskites at 5 K for (a) SL05, (b) SL15 and (c) SL25; the lower set of bars corresponds to the Bragg reflections of the magnetic phase.

Nèel temperature has been reported for Sr_2CoWO_6 [5]. A Curie–Weiss fit above 180 K gives paramagnetic moments of 4.71, 4.81 and 4.89 μ_B/f.u. for SL05, SL15 and SL25, respectively, whereas the corresponding Weiss temperatures of −80, −76 and −67 K confirm the presence of antiferromagnetic interactions in the paramagnetic regions.

The magnetic moment per unit formula calculated from the magnetic susceptibility data for the stoichiometries given above reveals that the increment of the magnetic ion in the 2*d* site is the responsible for the subtle observed variations. The magnetic moment per magnetic atom (4.64, 4.64 and 4.68 μ_B/atom for SL05, SL15 and SL25, respectively) indicates unquenched Co^{2+}(HS) with electronic configuration $Co^{2+}(3d^7)$–$W^{6+}(5d^0)$. The corresponding theoretical values are 3.87–6.63 μ_B for spin only and spin–orbit, respectively [21].

Although the coexistence of Co^{2+}/Co^{3+} as magnetic ion cannot be disregarded, our calculated values per magnetic ion result lower than those reported in the literature for non-doped similar systems with unquenched Co^{2+}(HS) whose effective moments are between 3.87 μ_B (spin only) and 5.20 μ_B (unquenched orbital contribution) [4,5,22,23].

Higher values should be found for Co^{3+} (HS) which exhibits 4.82−6.92 μ_B for spin only and spin–orbit, respectively [21,24,25].

Only in a few systems other authors claim the existence of Co^{3+} with intermediate spin in the *B* sites in simple perovskite ($LaCoO_3$) at low temperatures [25]. In our case, this fact is not observed and only Co^{2+} in both *B* sites is confirmed. W^{5+} (d^1) existence is also disregarded since no evidence of its paramagnetic behavior is observed in the susceptibility curves.

3.3. Magnetic structure

The magnetic structure of SL05, SL15 and SL25 were analyzed from a set of NPD patterns collected at 5 K, with $\lambda = 1.594$ Å. New peaks appear corresponding to magnetic satellites defined by the propagation vector $k = (\frac{1}{2}, 0, \frac{1}{2})$. An antiferromagnetic structure was modeled with magnetic moments at the Co positions; after the full refinement of the profile, including the magnetic moment magnitude, discrepancy factors of $R_{mag} = 9.69\%$, 12.1% and 14.6% were reached for the 5 K diagram for SL05, SL15 and SL25, respectively. The notation of the Co position of the Co atoms is Co1 (1/2,0,1/2) and Co2 (0,1/2,0). The solution corresponds to the following coupling between the magnetic moments: $m_{1x} = -m_{2x}$, $m_{1y} = -m_{2y}$ and $m_{1z} = m_{2z} = 0$.

The refined profile is shown in Fig. 7 and the final parameters and a list of the main interatomic distances and angles are shown in Table 3. A view of the magnetic structure is displayed in Fig. 8. The proposed magnetic arrangement gives rise to antiferromagnetic couplings between each Co moment and the six neighbors, via –O–W–O– paths in each phase. The magnetic structure can be alternately described as an array of ferromagnetic layers of Co moments, perpendicular to the [101] directions, coupled antiferromagnetically. The magnetic moments at 5 K are 2.15(1),

Table 3
Cell parameters, main bond distances (Å) and selected angles (deg) for monoclinic La-doped double perovskites $[Sr_{2-x}La_x]_{4e}[Co]_{2c}[W_{1-y}Co_y]_{2d}O_6$ from NPD data at 5 K

	SL05	SL15	SL25
Cell parameters			
a (Å)	5.60663(9)	5.60619(9)	5.6046(1)
b (Å)	5.58191(8)	5.58179(8)	5.5803(1)
c (Å)	7.8916(1)	7.8923(1)	7.8894(2)
β (deg)	90.038(4)	90.047(3)	90.051(4)
V (Å^3)	246.971(6)	246.970(6)	246.744(9)
CoO_6 octahedra			
Co–O1(×2)	2.076(4)	2.080(3)	2.066(4)
Co–O2(×2)	2.073(3)	2.071(3)	2.070(4)
Co–O3(×2)	2.061(3)	2.059(3)	2.061(4)
⟨Co–O⟩	2.069(2)	2.069(1)	2.066(2)
B″O_6 octahedra			
B″–O1(×2)	1.910(4)	1.910(3)	1.922(4)
B″–O2(×2)	1.927(4)	1.930(4)	1.928(4)
B″–O3(×2)	1.923(3)	1.926(3)	1.925(4)
⟨B″–O⟩	1.920(1)	1.922(1)	1.925(2)
Co–O1–B″(×2)	163.7(2)°	163.1(1)°	163.0(2)°
Co–O2–B″(×2)	162.9(1)°	162.7(1)°	163.0(2)°
Co–O3–B″(×2)	166.5(1)°	165.9(1)°	165.7(2)°
⟨Co–O–B″⟩	164.4°	163.9°	163.9°
AO_{12} polyhedra			
A–O1	2.913(3)	2.923(3)	2.915(3)
A–O1	2.703(3)	2.694(3)	2.700(3)
A–O1	3.075(2)	3.089(2)	3.088(3)
A–O1	2.537(2)	2.524(2)	2.522(3)
A–O2	2.737(6)	2.738(6)	2.727(6)
A–O2	2.546(6)	2.543(6)	2.548(7)
A–O2	3.127(6)	3.134(6)	3.122(7)
A–O2	2.805(6)	2.800(6)	2.813(7)
A–O3	2.799(7)	2.797(7)	2.798(7)
A–O3	3.082(6)	3.090(6)	3.095(7)
A–O3	2.587(6)	2.584(6)	2.572(7)
A–O3	2.730(6)	2.731(6)	2.733(7)
⟨A–O⟩	2.803	2.804	2.803

2.16(1) and 2.36(4) μ_B for SL05, SL15 and SL25, respectively. These values represent the magnetic moment per Co^{2+} ion in the ordered state and should be associated with the spin-only contribution, although it is lower than the expected value for high-spin Co^{2+} of 3 μ_B/atom, probably due to covalence effects.

4. Conclusions

We have prepared a series of mixed Co–W double perovskites of the type A_2CoWO_6 where *A* is Sr^{2+} doped with La^{3+}. In particular, we have settled how the structure responds to changes in the effective size and charge of the *A*-type site, using a combination of XRPD and NPD methods. The results of Rietveld analysis indicate the occurrence of a structural phase transition from a tetragonal ($I4/m$) lattice in Sr_2CoWO_6 to a monoclinic ($P2_1/n$) one from smallest grade of substitution. The doping in the *A* site for a higher charged cation did not led to an injection of electrons as it effectively occurs in systems with $B' = Fe$. However, an interesting structural change due to the re-ordering of the Co ions in different *B* sites has been found and also supported by the magnetic moment values per formula obtained for the determined stoichiometries. This modification is unprecedent since it has never been observed before in similar systems. Variable temperature NPD data do not show structural changes down to 5 K. NPD refinements at 5 K and magnetic measurements indicate a transition to an antiferromagnetic order state at $T_N = 24$ K.

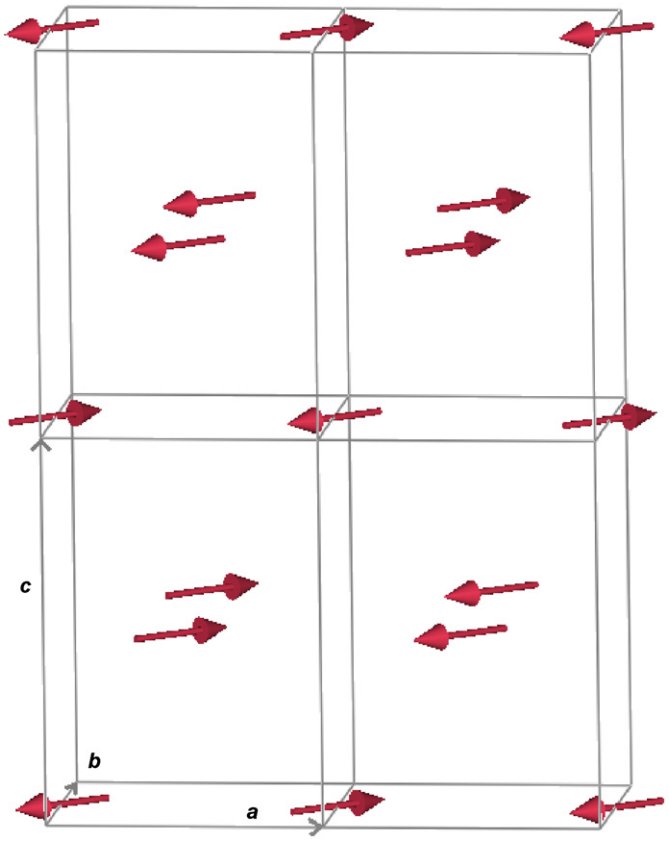

Fig. 8. Schematic view of the magnetic structure of the La-doped double perovskites. The chemical unit cell is doubled along *x* and *z*. Only Co ions and their magnetic moments oriented along (110 direction) are represented.

The results of the magnetic behavior are consistent with an electronic configuration $Co^{2+}(3d^7)$–$W^{6+}(5d^0)$ instead of $Co^{2+/3+}$ ($3d^7/3d^6$)–$W^{5+/6+}(5d^1/5d^0)$.

Acknowledgments

J.C.P. thanks ANPCyT (Project PICT 25459), SECyT-UNSL (Project 7707), and CONICET (PIP no. 6246). R.E.C. thanks ANPCyT (PICT2003 06-15102), CONICET (PIP 5767) and SECYT-UNC (197/05). J.C.P., R.D.S and R.E.C. are members of CONICET. We are grateful to ILL for making all facilities available.

References

[1] K.I. Kobayashi, T. Kimura, H. Sawada, K. Terakura, Y. Tokura, Nature 395 (1998) 677–680.
[2] D. Niebieskikwiat, R.D. Sánchez, A. Caneiro, L. Morales, M. Vásquez-Mansilla, F. Rivadulla, L. Hueso, Phys. Rev. B 62 (2000) 3340–3345.
[3] D. Niebieskikwiat, A. Caneiro, R.D. Sánchez, J. Fontcuberta, Phys. Rev. B 64 (2001) 180406.
[4] M.C. Viola, M.J. Martínez Lope, J.A. Alonso, P. Velazco, J.L. Martínez, J.C. Pedregosa, R.E. Carbonio, M.T. Fernández-Díaz, Chem. Mater. 14 (2002) 812–818.
[5] M.C. Viola, M.J. Martínez-Lope, J.A. Alonso, J.L. Martínez, J.M. De Paoli, S. Pagola, J.C. Pedregosa, M.T. Fernández-Díaz, R.E. Carbonio, Chem. Mater. 15 (2003) 1655–1663.
[6] P.M. Woodward, Acta Crystallogr. B 53 (1997) 32–43.
[7] D. Sánchez, J.A. Alonso, M. García-Hernández, M.J. Martínez-Lope, M.T. Casais, J.L. Martínez, J. Mater. Chem. 13 (2003) 1771–1777.
[8] J. Lindén, T. Shimada, T. Motohashi, H. Yamauchi, M. Karppinen, Solid State Commun. 129 (2004) 129–133.
[9] Q. Lin, M. Greenblatt, M. Croft, J. Solid State Chem. 178 (2005) 1356–1366.

[10] J. Navarro, J. Nogués, J.S. Muñoz, J. Fontcuberta, Phys. Rev. B 67 (2003) 174416.
[11] C. Frontera, D. Rubí, J. Navarro, J.L. García-Muñoz, C. Ritter, J. Fontcuberta, Physica B 350 (2004) E285–E288.
[12] D. Rubí, C. Frontera, G. Herranz, J.L. García-Muñoz, J. Fontcuberta, C. Ritter, J. Appl. Phys. 95 (2004) 7082–7084.
[13] C. Frontera, D. Rubi, J. Navarro, J.L. García-Muñoz, J. Fontcuberta, C. Ritter, Phys. Rev. B 68 (2003) 012412.
[14] H.M. Rietveld, J. Appl. Crystallogr. 2 (1969) 65–71.
[15] J. Rodríguez-Carvajal, Physica B 192 (1993) 55–69.
[16] Theo Hahn (Ed.), International Tables for Crystallography, vol. A, "Space-group Symmetry," Published for International Union of Crystallography (IUCr) by D. Reidel Publishing Company, Dordrecht, Holland, Boston, USA, 1983, p. 177.
[17] E. Guermen, E. Daniels, J.S. King, J. Chem. Phys. 55 (1971) 1093–1097.
[18] M.W. Lufaso, P.W. Barness, P.M. Woodward, Acta Crystallogr. B 62 (2006) 397–420.
[19] J.A. Alonso, M.T. Casais, M.J. Martínez-Lope, P. Velasco, A. Muñoz, M.T. Fernández-Díaz, Chem. Mater. 12 (2000) 161–168.
[20] J.B. Philipp, P. Majewski, L. Alff, A. Erb, R. Gross, T. Graf, M.S. Brandt, J. Simon, T. Walther, W. Mader, D. Topwal, D.D. Sarma, Phys. Rev. B 68 (2003), 14431-1–14431-13.
[21] J.S. Smart, Effective Field Theories of Magnetism, W.S. Saunders Company, Philadelphia, London, 1966.
[22] R.M. Pinacca, M.C. Viola, J.C. Pedregosa, A. Muñoz, J.A. Alonso, J.L. Martínez, R.E. Carbonio, Dalton Trans. 3 (2005) 447–451.
[23] V. Primo-Martín, M. Jansen, J. Solid State Chem. 157 (2001) 76–85.
[24] R.J. Radwanski, Z. Ropka, Physica B 507 (2000) 281–282.
[25] C. Zobel, M. Kriener, D. Bruns, J. Baier, M. Grüninger, T. Lorenz, P. Reutler, A. Revcolevschi, Phys. Rev. B 66 (2002), 020402-1–020402-4.